HIGH RESOLUTION RADAR MAPPING OF THE CIERVA POINT, ANTARCTIC

Jandyr M. Travassos[1], Jorge E. Musa[2] and Luis Peche[3]

ABSTRACT. The excellent penetration of the electromagnetic field in ice favors the radar and the radio-echo sounding methods for the study of ice masses laying on Earth's surface. In particular the ground penetrating radar has proved to be very effective for surface-based studies of land and sea ice. The most ubiquitous radar signatures are reflections from the internal structure of ice, the so-called stratigraphic layers, or from the bedrock. In this paper we concentrate on some reflection phenomena other than on ice stratigraphy revealed on the ice cover of the Cierva Point, Antarctic Peninsula. We acquired 25 SW-NE and NE-SE profiles in an area of 140 $\times$ 175 m^2 with an acquisition train of 2 Nansen sledges dragged by a ski-doo. Radar sections revealed internal reflection horizons are caused by changes in dielectric properties as well as density fluctuations and preferred crystal orientation fabric.

Keywords: GPR, radar stratigraphy, low reflectivity zone, Antarctic.

RESUMO. A excelente penetração do campo eletromagnético no gelo privilegia os métodos de radar e a radio-ecossondagem para o estudo das massas de gelo na superfície terrestre. Em particular o radar de penetração de solo tem provado ser efetivo em estudos de superfície em gelo terrestre e marinho. As principais características presentes nas seções de radar são as reflexões provenientes da estrutura interna do gelo, os níveis estratigráficos, ou seu embasamento rochoso. Neste trabalho nos concentramos em fenômenos distintos da estratigrafia revelados na cobertura de gelo da Ponta Cierva, na Península Antártica. Coletamos 25 SW-NE e NE-SE perfis em uma área de 140 $\times$ 175 m^2, com um trem de aquisição composto de 2 trenós Nansen tracionados por uma moto de neve. As seções de radar revelaram reflexões internas originadas por mudanças nas propriedades elétricas, na densidade do gelo e devido à orientação preferencial dos cristais de gelo.

Palavras-chave: GPR, estratigrafia, zona de baixa reflectividade, Antártica.

[1]Observatório Nacional, Rua General José Cristino, 77, São Cristóvão, 20921-400 Rio de Janeiro, RJ, Brazil. Phone/Fax: +55(21) 2580-7081 – E-mail: jandyr@on.br

[2]Universidade do Grande Rio, Rua General Canabarro, 165, 25 de Agosto, 25071-070 Duque de Caxias, RJ, Brazil. Phone/Fax: +55(21) 2672-7790 – E-mail: musa_62@yahoo.com

[3]Universidade do Estado do Rio de Janeiro/FGEL/DGAP, Rua São Francisco Xavier, 524, Maracanã, 20550-900 Rio de Janeiro, RJ, Brazil. Phone/Fax: +55(21) 2587-7102 – E-mail: peche@on.br

INTRODUCTION

The RES (radio-echo sounding) and the GPR (ground penetrating radar) are electromagnetic (EM) methods that have been extensively used for surface-based cryospheric studies for several decades (Walford, 1964). Applications have included measurements ice mass thickness, basal conditions, liquid water content, and ice internal structure. The form of internal reflection horizons, usually interpreted as isochronous horizons, reveals the stratigraphy of ice layers originated from the accumulating snow. Those are imaged radar discontinuities caused by changes in density, liquid water content, chemical impurities, crystal fabric, and structures as ice layers and glands within firn and glacial inclusions (air and/or water). Most works on GPR deal with ice stratigraphy (Arcone, 1996; Murray et al., 1997; Navarro et al., 2009), to determine accumulation rates by interpreting reflecting horizons, Forster et al. (1991); Kohler et al. (1997), anomalies in isochronous ice layers near ice dividers, Vaughan et al. (1999), and bed topography, Moran et al. (2000) and water contents (e.g., Bradford et al., 2009). Deep penetrating radar has been used to map the bedrock beneath glaciers and ice sheets to depths as great as several kilometers, e.g. Drewry et al. (1982); Bogorodsky et al. (1985). Those systems are operated on the ice surface or from an aircraft.

GPR has also been used for inferring the dielectric properties of near-surface snow, firn and ice that are important for interpreting SAR satellite images, Rott et al. (1993). In addition, GPR data can also be used to give direct measure of ice thickness, bedrock topography, and to display many internal reflections between the bedrock and ice surface due to small permittivity changes within the ice. Further, these studies can help the determination of the mass balance of ice sheets, which along with their size and dynamics are key issues in assessing the impact of global climate change on the cryosphere, Paterson (1994); Van der Veen (1991). Even large volcanic events may be detected in GPR sections Millar (1981).

This work presents GPR results obtained on Cierva Peninsula ice cap, Danco Coast, as part of a multi-institutional study employing different methodological approaches on the various indications for on-going climatic and glacial changes in the region, such as air temperature increase, changes in the precipitation regime. The snow covers can be used as indicators for climatic changes at a variety of temporal and spatial scales due to their short response times to climate changes.

FIELDWORK

Cierva Peninsula is located in the northwestern portion of the Antarctic Peninsula, on the south coast of Cierva Cove. Prima-

vera Base (Argentina) and its associated installations are located at Cierva Point on an ice-free area on its northern tip. The GPR survey was made on an area of 140 × 175 m² in the SW-NE and NE-SE directions, as shown in Figure 1. We have used a bi-static radar system, Pulse EKKO 100™, with 1000 V pulse and 100 MHz antennas in broadside perpendicular configuration with fixed distance of 1 m. Positioning was provided by a Leica DGPS 500, with the antenna mounted on a pole 2 m from ice surface. A second GPS unit was kept at Primavera Base to provide a post-processed accuracy of ±0.3 m in positioning and 1 m in height.
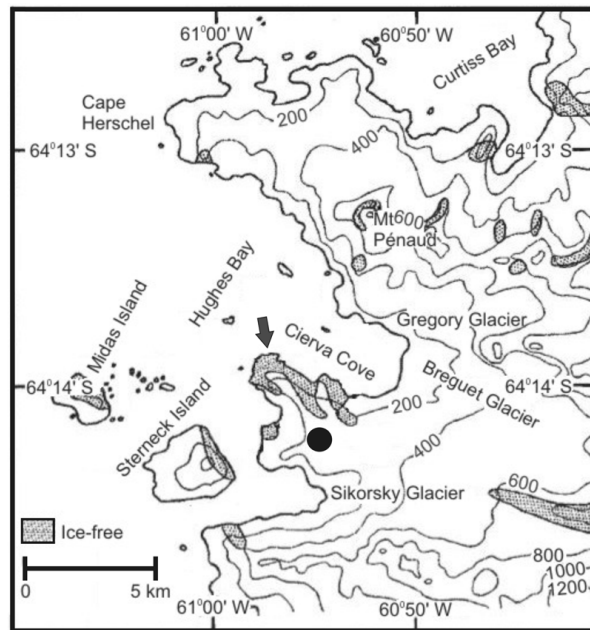

Figure 1 – Topographic map of Cierva Peninsula and environs. The study area, marked as a black filled circle, is on a plateau of about 250 m high between Peak Mojon (280 m) and Escombrera (323 m). The location of the Argentinean Base Primavera is arrowed. Map modified from Anonymous (1978).

Data were collected with an acquisition train of 2 Nansen sledges dragged by a ski-doo. The first Nansen sledge carried both the GPR and GPS systems and an operator, while the second held the antennas, 15 m away from the ski-doo, as shown in Figure 2. The antennas sat on the deck of the sledge, less than 0.3 m from ice surface thus imposing a certain degree of focusing to the EM field due to the permittivity contrast between air and snow. On the other hand the antennas are protected from ground irregularities on the deck.

We collected both fixed offset and CMP data. All the fixed offset data was collected with the acquisition train with automatic firing whereas the CMP data were collected by hand with manual firing. All the data had a time window of 2600 ns with a sampling

rate of 1 ns with a stack of 2 and 8 for the train and CMP, respectively. Those acquisition parameters together with the minimum manageable towing speeds of about 10 km/h limited the spatial sampling rate to about 2 m. The final sampling rate is based on the continuous data acquisition adjusted to the DGPS profile, see below.
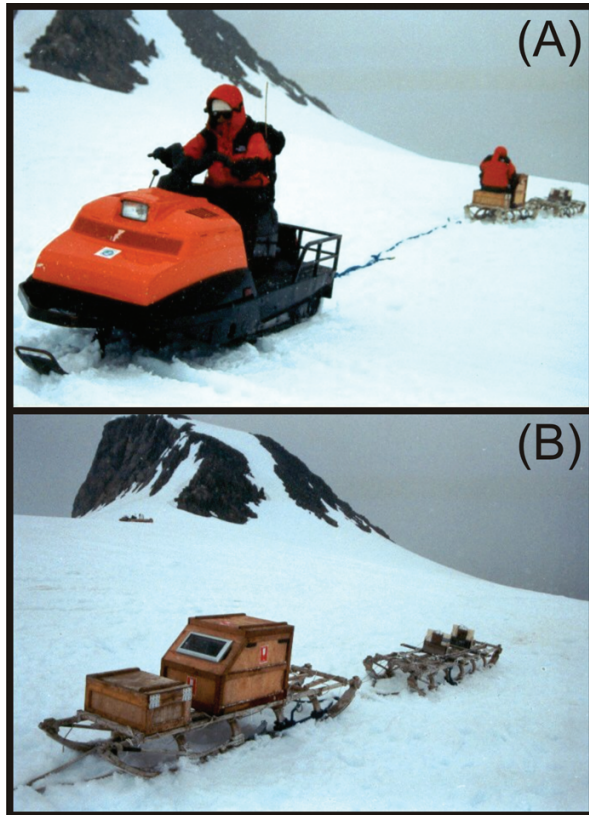

Figure 2 – The acquisition train used in the fieldwork. The first Nansen sledge carries the GPR and GPS systems and an operator (one of the authors, JMT). The second sledge carries the antennas, 15 m away from the ski-doo. Panel A shows the entire acquisition train. Panel B provides a zoom on the two sledges, with Peak Mojon (280 m) on the background.

DATA PROCESSING

The GPR firing was automatic and independent of the GPS positioning. The control on the speed of the acquisition train relied entirely on the driver's ability of keeping a route and judge the ski-doo speedometer at the same time. No wonder how difficult that was in a white area. All that conspired to a wildly varying trace spacing for the GPR profiles making the trace positioning a painstaking task. An automatic numerical procedure was written to position all traces correctly.

Trace positioning was followed by discarding all traces but those acquired with a fairly constant velocity of the acquisition train. All data segments obtained while speeding up to a given

cruise speed were discarded. So were those segments where the acquisition train was grinding to a halt. We have also discarded all data segments subject to expressive angular acceleration, what has resulted in fairly straight profiles. Moreover as most of the data acquisition was done in a zigzag fashion each second profile has to be reversed so as all profiles along a given direction will run with the same sense of way. In the end of this process of processing the geometry we have ended up with 20 profiles running SW-NE and 5 NE-SE profiles. The average lengths were 140 m and 200 m, respectively. The 25 fixed-offset profiles are shown superimposed on the topographic map of the study area, Figure 3.
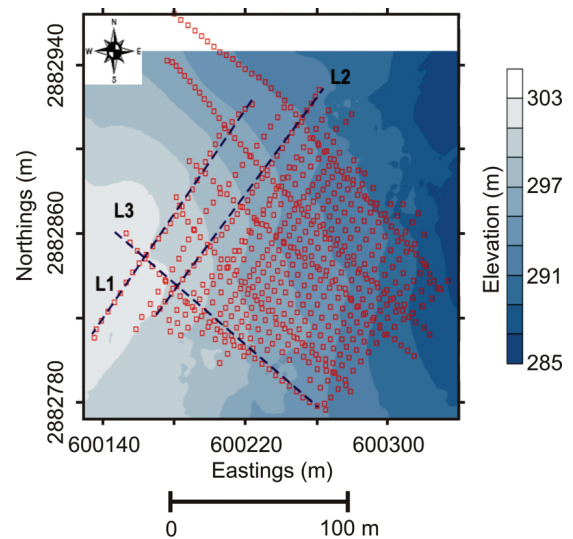

Figure 3 – All 25 fixed-offset profiles superimposed on the topographic map of the study area. Profiles appear as series of red squares equally spaced in time, so that their mutual distance reflect velocity variations on the field. The three profiles L1, L2 and L3, referred to in this paper are highlighted as dashed blue straight line segments.

Once all traces were correctly positioned we have made trace spacing uniform along all profiles by linear interpolation and spatial filtering. We have chosen a step size greater than the mode to keep trace extrapolation negligible: 2.25 m. An anti-aliasing spatial filter of 90% of the corresponding Nyquist yielded a theoretical lower limit to the spatial sampling of 0.2 cycles/m. That results in an image with a lateral degree of smoothing on the order of 5 m for earlier time and well over that at later times.

Data were dewowed and exponentially gained to compensate for losses. The attenuation factor used for the gain was estimated from the average trace envelope. Data were then band-pass filtered (40 and 160 MHz) and AGC gained afterwards. As the survey area was not flat we made topography correction to the data prior to migration.

A CMP profile in the area produced a two-velocity model: $v_1 = 0.09$ m/ns for TWT ≤ 198 ns and $v_2 = 0.12$ m/ns to the end of the time window. Figure 4 displays the velocity model superimposed on the semblance analysis panel. We have tried several migration velocities starting with the velocity model above and found that a single migration velocity of $v_m = 0.1$ m/ns yielded a good result. All profiles were then migrated with that migration velocity.
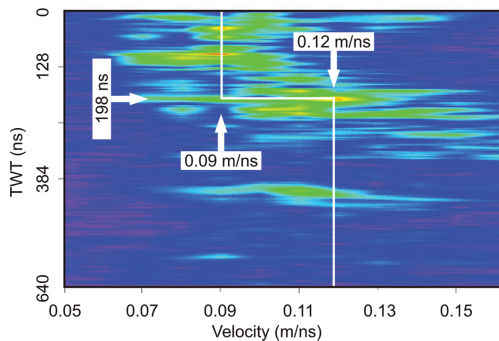

Figure 4 – The velocity model superimposed on a semblance analysis panel obtained from a CMP profile. In this and the next figures TWT is two-way travel time in ns.

RESULTS

In this paper we are going to concentrate in 3 profiles that illustrate the most important features of our data set. Two of those, L1 and L2, run SW-NE while the third, L3, run NE-SE, please refer to Figure 3. Those three lines are shown in Figures 5, 6 and 7, respectively. Sections show fairly horizontal reflectors and a conspicuous low reflectivity zone (LRZ) roughly spanning from 300 to 600 ns, or from 16 to 28 m. That zone, LRZ for short, probably is a result of a change of macroscopic change in permittivity due to microscopic changes at crystal level (Fujita et al., 2006) is followed by a horizon of stronger reflections associated to bedrock, between 600 and 800 ns (28 to 40 m). The region between 0 and 240 ns is related to snow and corresponds to velocity v_1 seen in CMP-derived velocity model.

The LRZ is probably caused by a change in crystal orientation from a random to a preferred angular distribution due to ice stress. It appears at the highest ground of our study area, Figure 3, towards Peak Mojon (280 m), seen in the background of Figure 2. In all three profiles the LRZ ends at the bedrock.

The LRZ and the bedrock are the most important features in our data set, spanning from roughly 200 to 600 ns. We can map the areal extent of the LRZ by analyzing a time slice of the averaged enveloped amplitude from 194 to 388 ns. The LRZ is seen at the western corner of our survey area, as shown in Figure 8. The high reflectivity zones seen in Figure 8 are attributed to strong reflecting ice structures.
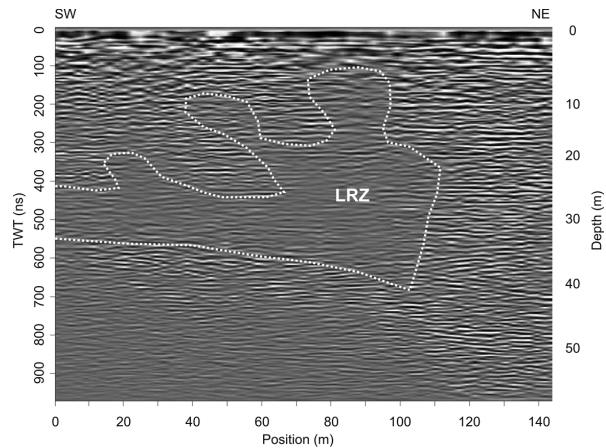

Figure 5 – Fixed-offset section of profile L1, see Figure 3, displaying fairly horizontal reflectors and a conspicuous low reflectivity zone (LRZ). Early time data ($\leq$100 ns) appears aliased due to the spatial sampling.

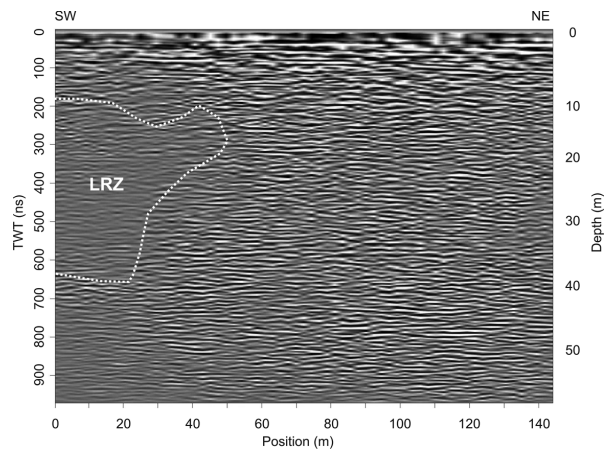**Figure 6** – Fixed-offset section of profile L2, see Figure 3, displaying fairly horizontal reflectors and a conspicuous LRZ. Early time data ($\leq$ 200 ns) appears aliased due to the spatial sampling.
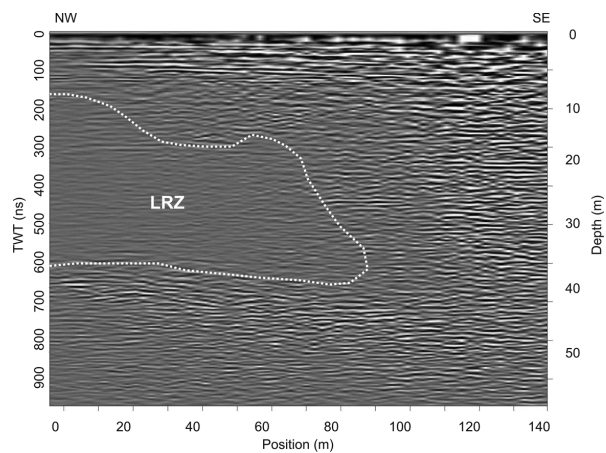

Figure 7 – Fixed-offset section of profile L3, see Figure 3, displaying fairly horizontal reflectors and a larger conspicuous LRZ. Early time data ($\leq$ 100 ns) appears aliased due to the spatial sampling.
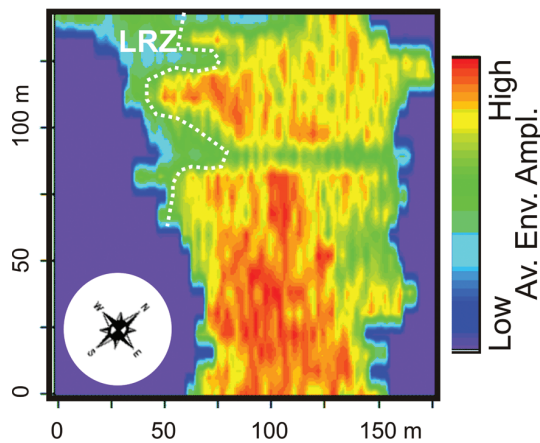
Figure 8 – Time slice of the averaged enveloped amplitude spanning from 194 to 388 ns of the SW-NE fixed-offset profiles. The LRZ is seen at the northwestern corner of the survey area.

CONCLUSIONS

In this paper we have studied the ice cover of the Cierva Point in the northwestern portion of the Antarctic Peninsula, using an 100 MHz GPR. We have surveyed an area of 140 × 175 m² with 25 SW-NE and NE-SE profiles. The fixed-offset profiles data were collected with an acquisition train composed of 2 Nansen sledges dragged by a ski-doo with differential GPS positioning. The GPR and GPS data were collected independently turning trace positioning the most time-consuming task in the processing stage.

We analyzed a small selection of our larger data set, comprising of 3 profiles that illustrate the most important results. Radar sections show fairly horizontal reflectors and a conspicuous low reflectivity zone roughly spanning from 300 to 600 ns, or from 16 to 28 m at the NW corner of the study area. That LRZ is probably a result of a change of macroscopic change in permittivity due to microscopic changes at crystal level (Fujita et al., 2006) is followed by a horizon of stronger reflections associated to the bedrock, between 600 and 800 ns (28 to 40 m). The region between 0 and 240 ns is related to snow and corresponds to velocity v_1 seen in CMP-derived velocity model.

The data displays a strong data acquisition footprint, being heavily averaged along profiles. In any case the data is characterized by the absence of isochronous due to the fast movement of the ice mass. That comes hardly as a surprise as the survey area is not a glacier nor an ice cover but rather a snow-firn cover on a strong topography. On the other hand the radar sections revealed internal reflection horizons caused by changes in dielectric properties due to density fluctuations and preferred crystal orientation fabric. One preeminent feature was a LRZ characterized by very weak reflectors, occurring before the EM waves reached the bedrock. This change of the crystal orientation fabric

can be a response to stress due to the ice movement induced by the bed topography.

REFERENCES

ANONYMOUS. 1978. Management Plan for Antarctic Specially Protected Area No. 134. The National Science Foundation document NSF 01-151. Available at: <http://www.nsf.gov/od/opp/antarct/aca/nsf01151/start.jsp>. Access on: May 2, 2008.

ARCONE SA. 1996. High resolution of glacial ice stratigraphy: a ground-penetrating radar study of Pegasus Runway, McMurdo Station, Antarctica. Geophysics, 61: 1653–1663.

BOGORODSKY VV, BENTLEY CR & GUDMANDSEN PE. 1985. Radioglaciology. Dordrecht: Reidel, 254 pp.

BRADFORD JH, NICHOLS J, MIKESELL TD & HARPER JT. 2009. Continuous profiles of electromagnetic wave velocity and water content in glaciers: an example from Bench Glacier, Alaska, USA. Ann. Glaciol., 50: 1–9.

DREWRY DJ, JORDAN SR & JANKOWSKI E. 1982. Measured properties of the Antarctic ice sheet: surface configuration, ice thickness, volume and bedrock characteristics. Ann. Glaciol., 3: 83–91.

FORSTER RR, DAVIS CH, RAND TW & MOORE RK. 1991. Snow-stratification investigation on an Antarctic ice stream with an X-band radar system. J. Glaciology, 37(127): 323–325.

FUJITA S, MAENO H & MATSUOKA K. 2006. Radio-wave depolarization and scattering within ice sheets: a matrix-based model to link radar and ice-core measurements and its application. J. Glaciol., 52(178): 407–424(18).

KOHLER J, MOORE JC, KENNET M, ENGESET R & ELVEHOY H. 1997. Using ground-penetrating radar to image previous years' summer surfaces for mass balance measurements. Ann. Glaciol., 24: 355–360.

MILLAR DHM. 1981. Radio-echo layering in polar ice sheets and past volcanic activity. Nature, 292: 441–443.

MORAN ML, ARCONE SA & DELANEY AJ. 2000. Delineation of a temperate glacier bed using 3-D migration. Proceedings of the Eighth International Conference on Ground Penetrating Radar (GPR 2000). SPIE, 4084: 236–242, Gold Coast, Australia.

MURRAY T, GOOCH DL & STUART GW. 1997. Structures within the surge front at Bakaninbreen, Svalbard, using ground-penetrating radar. Ann. Glaciol., 24: 122–129.

NAVARRO FJ, OTERO J, MACHERET YUYA, VASILENKO EV, LAPAZARAN JJ, AHLSTRØM AP & MACHÍO F. 2009. Radioglaciological studies on Hurd Peninsula glaciers, Livingston Island, Antarctica. Ann. Glaciol., 50: 17–24.

PATERSON WSB. 1994. The Physics of Glaciers. Elsevier, Oxford, 480 pp.

ROTT H, STURM K & MILLER H. 1993. Active and passive microwave signatures of Antarctic firn by means of field measurements and satellite data. Ann. Glaciol., 17: 337–343.

VAN DER VEEN CJ. 1991. State of balance of the cryosphere. Rev. Geophys., 29: 433–455.

VAUGHAN DG, CORR HFJ, DOAKE SM & WADDINGTON ED. 1999. Distortions of isochronous layers in ice revealed by ground-penetrating radar. Nature, 398: 323–326.

WALFORD MER. 1964. Radio echo sounding through an ice shelf. Nature, 204(4956): 317–319.

NOTES ABOUT THE AUTHORS

Jandyr de Menezes Travassos. Graduate in Physics from the Federal University of Rio de Janeiro (1976), Masters in Geology from the University of Rio de Janeiro (1981) and PhD in Geophysics – University of Edinburgh (1987). Actually is researcher of the National Observatory (U-III). With interest in fields of geophysics, with emphasis on Applied Geophysics, acting on the electromagnetic methods with application to model sedimentary basins, GPR (Ground Penetrating Radar) application with the analogous reservoirs and contamination of subsurface gasoline. It also develops research investigating the response of the cryosphere to global changes.

Jorge Elias Musa Carballo. Graduation in Physics – Universidad de La Habana (1992) and Ph.D. in Physics from the Brazilian Center for Physics Research (1999). Area of interest in condensed matter physics: production and characterization of ceramics, superconductivity, magnetism. From 2005 to 2008 he was researcher (post-doc) at the National Observatory where he worked in the area of data processing in Near Surface Geophysics.

Luis Alberto Peche Puertas. Graduate in Physics from the Universidad Nacional de Ingeniería (1993) Lima-Peru, Masters in Physics from the Brazilian Center for Physics Research (1998) and Ph.D. in Physics from Catholic University of Rio de Janeiro (2004). Since 2005 until 2009 he was researcher (post-doc) in National Observatory where he developed research in Applied Geophysics. His work has focused on the detection of contamination (gasoline) in the subsurface by analyzing the spectral attributes of the GPR trace, and worked on other problems such as the EM field propagation in waveguides and imaging of the cryosphere. He is currently a Visiting Professor at the Faculty of Geology of the State University of Rio de Janeiro (UERJ), focusing interest in the area of seismic data processing and GPR.